

Three-dimensional data of wirecut surface scans under the confocal microscope (110 character maximum, inc. spaces)

Yuhang Lin^{1,2,*}, Heike Hofmann^{2,3}, Curtis Mosher⁴, Eden Amin⁵, Jeff Salyards², and Alicia Carriquiry^{1,2}

¹Iowa State University, Department of Statistics, Ames, IA, 50011, USA

²Iowa State University, Center for Statistics and Applications in Forensic Evidence, Ames, IA, 50011, USA

³University of Nebraska-Lincoln, Department of Statistics, Lincoln, NE, 68583, USA

⁴Iowa State University, Roy J Carver High Resolution Microscopy Facility, Ames, IA, 50011, USA

⁵University of Central Oklahoma, Forensic Science Institute, Edmond, OK, 73034, USA

*corresponding author(s): Yuhang Lin (yhlin@iastate.edu)

ABSTRACT

Update later: max of 170 words: describe the study, the assay(s) performed, resulting data, and reuse potential

Wire cut data is important in forensic investigations but lacks a systematic way of analyzing the data. We created a dataset of 120 scans of aluminum wire cut in $\times 3p$ format, using 5 wire cutters and 3 locations along the 4 blades, with 2 replicates for each combination. A systematic pipeline with multiple analysis plots was developed to analyze the data and draw conclusions based on numerical measures.

Background & Summary

Grammally safe to use, gpt safe to correct grammar and word, no new content

An important aspect of forensic analysis involves investigating marks left at crime scenes. Forensic examiners focus particularly on identifying the origin of these marks, a process known as the Source Identification Problem in Forensic Science¹. The forensic science community generally distinguishes between the **specific source problem**, where the examiner seeks to determine whether a mark was left by a particular tool, and the **common source problem**, which focuses on whether two marks were left by the same tool. Currently, accepted practice in both of these two problems relies on visual inspection of the items under a comparison microscope. The results, according to the Theory of Identification² developed by the Association of Firearm and Toolmark Examiners (AFTE), are categorized by examiner into three types: *identification*, where the marks are believed to have been made by the same source; *elimination*, where the marks are believed to have been made by different tools; and *inconclusive*, where similarities or dissimilarities between the marks are insufficient to allow either an identification or an elimination. However, this assessment is inherently subjective, which has led to criticism from reports by the National Research Council (NRC)³ and the President's Council of Advisors on Science and Technology (PCAST)⁴ for lacking quantifiable measures of objectivity and the absence of error rates. Such limitations highlight the need for empirical datasets with known ground truth to validate conclusions. Addressing this gap requires a structured approach that not only evaluates examiner performance but also considers case-specific evidence in a measurable way. To bridge this gap, it is necessary to establish a framework that integrates both empirical validation of examiner performance and measurable analysis of case-specific evidence. A crucial aspect of this framework is recognizing different methodological perspectives in forensic science.

In this context, Biedermann⁵ differentiates between internal and external perspectives in the forensic literature. The external perspective only allows general statements based on (black-box) studies relating examiners' conclusions to ground truth without considering any evidence of a particular case. To allow an internal perspective, there is a need to quantitatively capture the basis for an evaluation based on specific evidence. To transition toward an internal perspective, similarity comparisons are needed. However, no publicly available dataset currently exists for wirecut marks. The closest work is by Baiker et al.⁶, which focuses on screwdriver toolmarks, not wire cutters. Thus, there is an urgent need to collect and analyze public datasets specific to wirecut marks.

Understanding the characteristics of toolmarks left by wire cutters is essential. When a bladed tool cuts a wire, it leaves striations on the cut surface, as shown in Figure 1. These striations serve as evidence to assess the similarity. There have been



Figure 1. Microscopic close-up of striations left by a blade on the cut end of a wire.

42 cases where the evidence and testimony on wire cut evidence played a crucial role in the criminal investigation and conviction
43 of a defendant. However, forensic analysis of these evidence lacks a standardized quantitative approach, except for visual
44 comparisons.

45 A growing of research has sought to develop quantitative methods for analyzing forensic toolmarks, particularly those
46 created by different types of tools. Prior studies on striated toolmarks provide insights into key comparison factors, including
47 angle of attack⁶, rotational axis⁷, and cutting direction⁸. Foundational research in forensic toolmarks has emphasized dataset
48 collection and computational analysis. Ma et al.⁹ and Zheng et al.¹⁰ focused on collecting and distributing datasets for bullet
49 and toolmark analysis for this purpose. Chu et al.¹¹ and Vorburger et al.¹² demonstrated numerical methods for improving
50 accuracy and consistency. Hare et al.¹³ and Ju et al.¹⁴ developed similarity quantification techniques, but alignment remains
51 a major challenge.

52 In this study, we build on these methodologies to provide a publicly available dataset of wirecut scans, develop a sys-
53 tematic pipeline to analyze the data quantitatively, and introduce numerical measures for similarity assessment beyond visual
54 inspection. The dataset includes multiple types of files, as summarized in Table 1.

55 In github README: [renv folder](#) and [file](#) provide a technical way to ensure reproducibility in R. In this paper: Folder
56 variability-assessment contains documents for technical validations, the inner structure is mimicing the structure of the main
57 data folder.

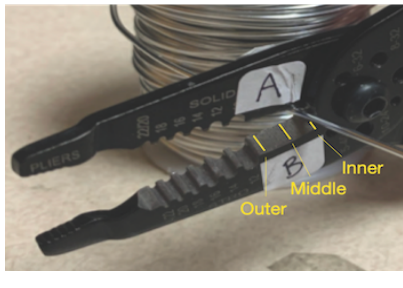
58 To ensure full reproducibility, we describe each step in detail, including how we collected and processed the wirecut
59 samples in [Cutting Wires](#) hyperlink location incorrect for unnumbered sections it seems that the hyperlinks make sure that the
60 section is on the page, profile extraction from scanned surfaces in [Extract Profiles](#) how we extract profiles from the scans,
61 filtering signals from profiles in [Filtered Signals](#), and alignment methodologies using the cross-correlation function (CCF) in
62 [Align Signals](#). The details regarding dataset hosting are discussed in [Data Records](#). A technical validation of consistency
63 of assumptions and conclusions is provided in [Technical Validation](#). [Usage Notes](#) includes open-source code for dataset
64 generation and analysis, as discussed in [Methods](#) and [Technical Validation](#). Finally, in [Code availability](#), we discuss access to
65 our code for reproducibility and future research. We anticipate that this dataset and analysis pipeline will serve as a foundation
66 for forensic practitioners and be extended to real-world crime scene investigations involving wirecut evidence.

67 Methods

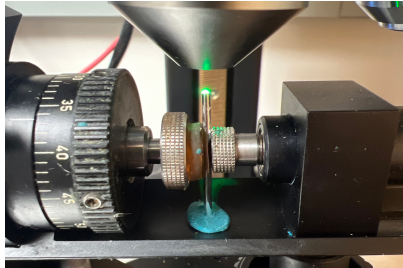
68 In this study, we use aluminium wire [more details: thickness, brand?](#) to create cuts. The physical property of aluminum wire
69 makes it an excellent candidate for keeping marks while being relatively easy to bend and non-toxic, i.e. with a hardness of
70 XXX aluminium is soft enough that tools leave marks, but hard enough to not be affected by handling cut materials under the
71 microscope.

Table 1. Structure of available data and files.

	Description	Section
Raw data		
scans/	folder containing 120 topographic 3d scans	Cutting Wires
meta.csv	corresponding to 30 aluminum wire cuts (x3p format) meta information for each cut with tool, blade, and location information (CSV format)	Cutting Wires
Manual derivatives		
profiles/	folder of files with manually extracted profiles (CSV format)	Extract Profiles
Computational derivatives in folder 'data-derived/'		
wire-signals	signals processed from corresponding profile (zipped CSV format)	Filtered Signals
wire_pairwise_ccf	CCF values of all pairwise aligned signals (zipped CSV format)	Align Signals
Image files		
pngs/	folder containing pictures of 3d scans of wire cuts (PNG format)	Cutting Wires
profile-images/	folder containing pictures of profile extracted from wire cuts (PNG format)	Extract Profiles
Visual Inventory in folder 'assessment/analysis-manual/'		
processing-wires	display of pairwise aligned signals from the same sources (HTML format)	Align Signals



(a)

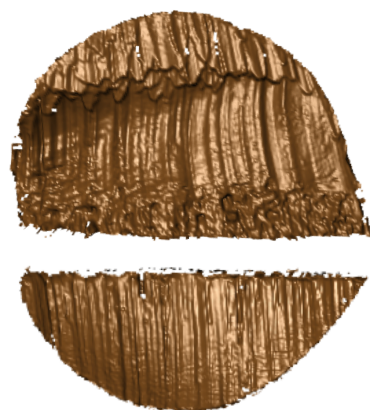


(b)

Blade A



Blade C



Blade B

(c)

Blade D

Figure 2. (a) A Kaiweets wire cutter of model KWS-105 was used to cut the wire, with inner, middle and outer locations marked. (b) A confocal microscope was used to scan the wire surfaces. (c) After separating 2 tent structures by the connecting position, we obtained 4 samples - 2 samples from blade A and B, and others from blade C and D. width and height are tuned manually | full requirements see <https://www.nature.com/sdata/publish/submission-guidelines#figures>

72 XXX look up the hardness value of aluminium, copper and lead. In real casework, aluminium wires are not seen as often
73 as lead or copper. We avoided using lead in the laboratory setting, because of its toxicity.

74 Cutting Wires

75 The aluminum wire used was 16 Gauge/1.5 mm, anodized. In order to cut the wire, 4-inch pieces were unspooled and cut
76 using Kaiweets wire cutters, model KWS-105, as shown in Figure 2a, for 1 blade location, either inner, middle, or outer, which
77 gives us 1 replicate. Each piece was then cut into half to create 2-inch pieces for each side, AB and CD, with a sharpie line
78 marking the cut ends, giving us 4 samples. Then, we use the standard scanning protocols for the confocal microscope, shown
79 in Figure Figure 2b, to scan the wire tip surfaces. The scanned surfaces are saved in a resolution of $0.645\mu m \times 0.645\mu m$ per
80 square pixel in an $\times 3p$ file format. Here, we are showing AB and CD sides in Figure 2c, with the back of A being C and
81 the back of B being D. Both AB and CD sides form tent structures on the tips of the wire, and we separate each side of the
82 tent into 2 pieces along the bending position, resulting in 8 scans. We repeated this process for all 3 locations along the blade
83 and 5 wire cutters, with 2 replicates for each tool-edge-location combination, resulting in 120 scans. Each piece was labeled
84 with the naming conventions, T(ool) 1/2/3/4/5 (Edge) A/B/C/D W(ire) - L(ocation) I(nner)/M(iddle)/O(uter) - R(epetition)
85 1/2, with T1AW-LI-R1 being the piece cut by tool 1 on the A edge at the inner location for the first repetition.

86 Extract Profiles

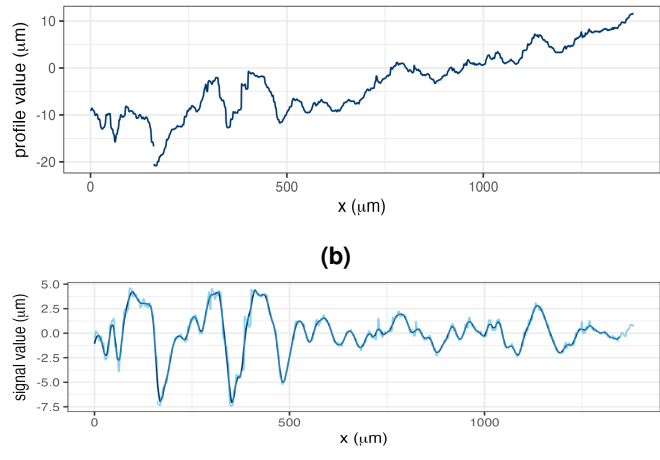
87 Numerical comparisons between 2 replicates cannot be done directly on the $\times 3p$ files. We need to extract representative
88 functions from the scans first. A representative function with the most information is considered as a signal for one scan,
89 which is used later for comparison. To obtain this function, we first need a profile of the scan, which is a sequence of values
90 along a user-drawn line on the surface. The profile captures most features of the scan and be orthogonal to the striation marks
91 of the scan, which are formed by the ups and downs of grooves. So, we draw the line across the wide region of the scan to
92 maximize the feature captured, as shown in dark blue in Figure 3a. We then investigate the values under this profile line. The
93 profile function along the line is plotted in Figure 3b.

94 Filtered Signals

95 With the profile extracted, we then obtain the signal. Two Gaussian filters, as discussed in Cleveland et al.¹⁵, are applied to
96 these resulting profiles. In particular, we first used a large low-pass filter with bandwidths of 400 microns to remove the large
97 trend, as it overwhelms the signals, and then used a small high-pass filter of 40 microns to average across noise and remove
98 spikes, as shown in Figure 3c. Finally, the extreme tail values are removed.



(a)



(b)

(c)

Figure 3. (a) A profile line in dark blue was drawn across the striations of the scan. (b) The profile function extracted along the profile line in (a). (c) The raw signal in light blue is obtained by using the low-pass filter on the profile function in (b) and the filtered signal is obtained by using the high-pass filter on the raw signal.

99 Align Signals

100 Signals extracted from different scans are put together for comparison, and we maximize the cross-correlation function (CCF)
 101 values between the signals to find the best alignment numerically. For example, we compare T1AW-LI-R1 to T1AW-LI-R2,
 102 T1CW-LI-R1 to T1CW-LI-R2, and so on. That is comparing each row in Figure 4. We know that signals from two replicates
 103 with the same tool-edge-location combination yield similar signals as in the first and second columns of Figure 5, which results
 104 in alignments of massive overlapping and high CCF values close to 1. The alignments and values we got in the rightmost
 105 column of Figure 5 fulfill our expectations.

106 Data Records

107 The complete dataset is available on the ISU DataShare repository at <https://iastate.figshare.com/>, which is public and open
 108 access for every interested researcher. The structure of the dataset is described before in Table 1.

109 Technical Validation

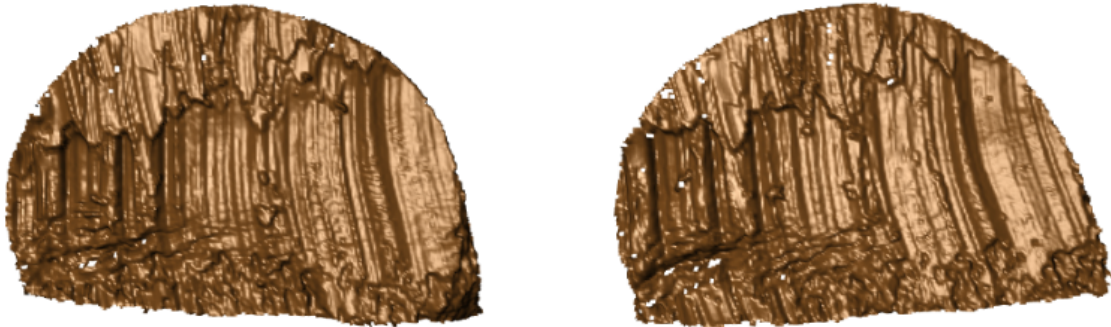
110 We conducted technical validation in different aspects, including validating the data collection process, processing scans and
 111 alignment of signals, and variability assessment.

112 The first validation we did lies in the data collection process. We have two team members did the cutting and labeling
 113 together, and the one person did the scanning and named according to the naming convention introduced in [Cutting Wires](#).
 114 The scanning was done in a specific order to ensure consistency across all scans. The data was saved in a consistent format to
 115 ensure easy access for analysis. A third person checked the data to ensure everything was correct and accurate.

116 The validation for processing scans and alignment of signals was conducted in the following manner. For the CCF scores
 117 calculated, we assume large scores between signals from the same source, and low scores between signals from different
 118 source. Figure 5 shown in [Align Signals](#) before matches our thought for signals from the same source. For different source,
 119 we take T1AW-LI-R1 and T2AW-LI-R1 as an example, as shown in Figure 6a and Figure 6b. The alignment is shown in
 120 Figure 6c with a 0.2 CCF value, which is low, as expected. We also put resulting CCFs for all pairwise comparisons in the
 121 boxplot, together with the receiver operating characteristic (ROC) curve, as in Figure 7 and Figure 8. The CCF values for the
 122 same sources are close to 1, while the CCF values for different sources are much lower than expected. This is consistent with
 123 our expectations and validates our pipeline for processing scans and alignment of signals.

124 The other validation we did is to assess the variability of our results. In particular, we assess the variabilities in different
 125 replicates, different staging and different acquisition. We arbitrarily picked scans from tool 2 at location middle for this
 126 assessment. The variability in different replicates can be seen as we took two different cuts on the same edge and same
 127 position, and it is fully discussed in previous comparison as Figure 5 shown in [Align Signals](#). For staging, we obtained the

Edge A



Edge C



Edge B



Edge D



Figure 4. Scans from different sides of tool 1 at the inner location.

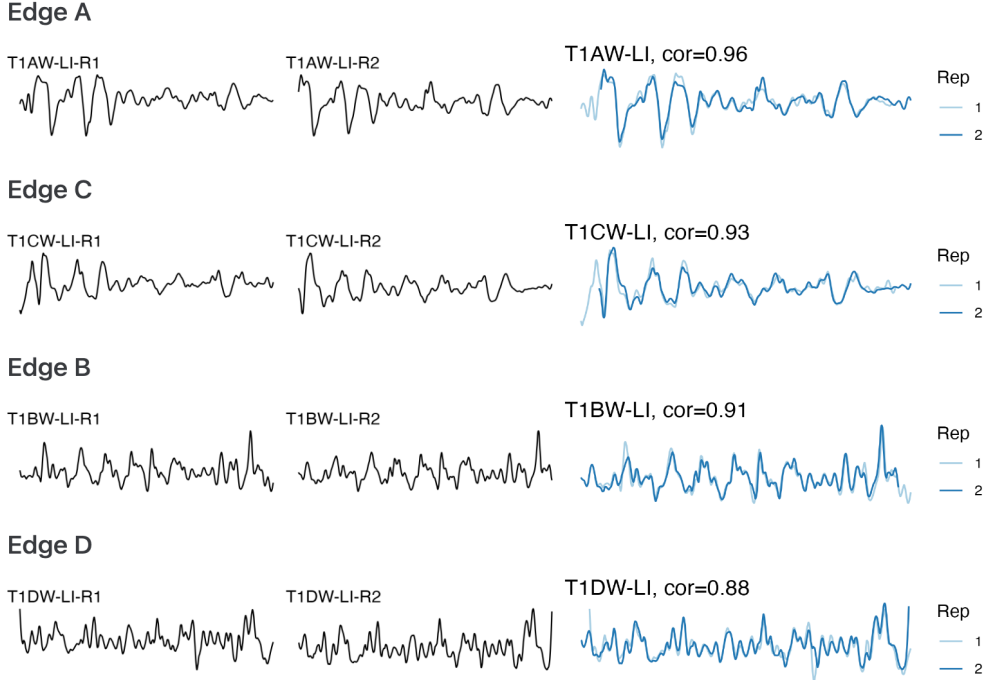


Figure 5. The first and second columns show the signals extracted from Figure 4, and the third column shows the alignments and CCF values between pairs of signals.

Table 2. Comparison of CCF across different settings.

Edge	Replicate (R)		Staging (S)			Acquisition (A)		
	Avg _R	SD _R	Avg _S	SD _S	Avg _S - Avg _R	Avg _A	SD _A	Avg _A - Avg _S
A	0.818	0.015	0.961	0.012	0.143	0.992	0.003	0.031
B	0.879	0.031	0.922	0.042	0.043	0.939	—	0.017
C	0.841	0.022	0.952	0.021	0.111	0.959	—	0.007
D	0.797	0.011	0.966	0.017	0.169	0.986	—	0.020

average CCF between replicates (replicate 1 and replicate 2) through pairwise comparison. Then, we rescanned replicate 2 under the confocal microscope, introducing a new staging labeled as S. Staging 1 for replicate 2 is omitted in the label, resulting in R2(-S1). For all four edges of tool 2 at location middle, we created three different stagings: R2, R2-S2, and R2-S3, and computed the average CCF between stagings using pairwise comparison.

Within each staging, we further examined the effect of different acquisitions by keeping the scans on the confocal microscope under varying lighting conditions, introducing a new acquisition label as A. For edge A at staging 3, we performed four acquisitions in total, omitting the first one in the label again, resulting in R2-S3(-A1). For the other three edges, we conducted two acquisitions in staging 3, denoted as R2-S3 and R2-S3-A2. The average CCF between acquisitions was then obtained through pairwise comparison.

With this setup, we expect increasing consistency in the CCF from replicate to staging to acquisition, as conditions become progressively more stable. Consequently, variability should decrease along this sequence. We also computed the differences between replicate, staging, and acquisition, expecting smaller differences between acquisition and staging compared to those between staging and replicate. We can visualize the results as scatter plots, as shown in Figure 9. The interval within 2 SD is also shown. There is an increase in the average as shown as orange bar and a decrease in standard deviation (SD) as shown in the interval width in the plot. The detailed numeric results, together with standard deviation and differences in averages, shown in Table 2, confirm our expectations.

While the difference between the order of profiles extracted and the person who extracted the profile remains another huge area for research, we leave that for further discussion.

Check if vertical lines are allowed. if not, add empty columns between E / R / S / A.

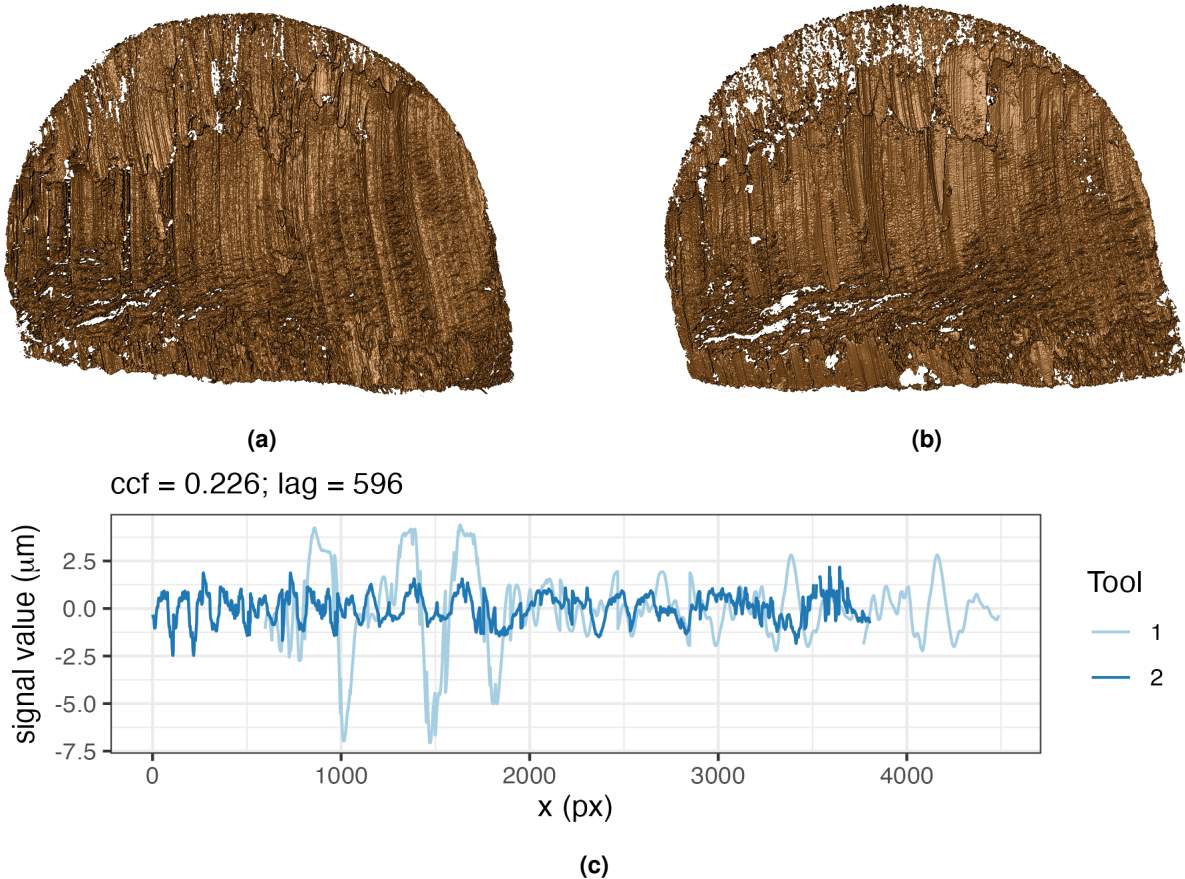


Figure 6. (a) Scan T1AW-LI-R1 cut by tool 1. (b) Scan T2AW-LI-R1 cut by tool 2. (c) Alignment of signals from T1AW-LI-R1 and T2AW-LI-R1.

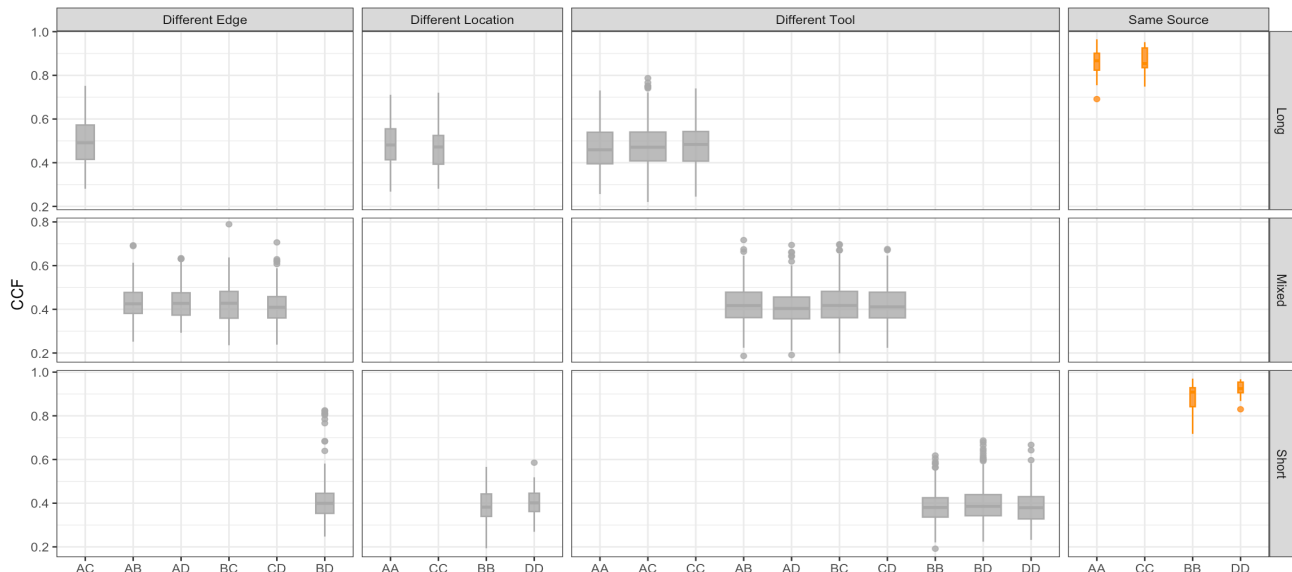


Figure 7. The boxplot shows that signals from the same sources have higher CCFs than those from different sources.

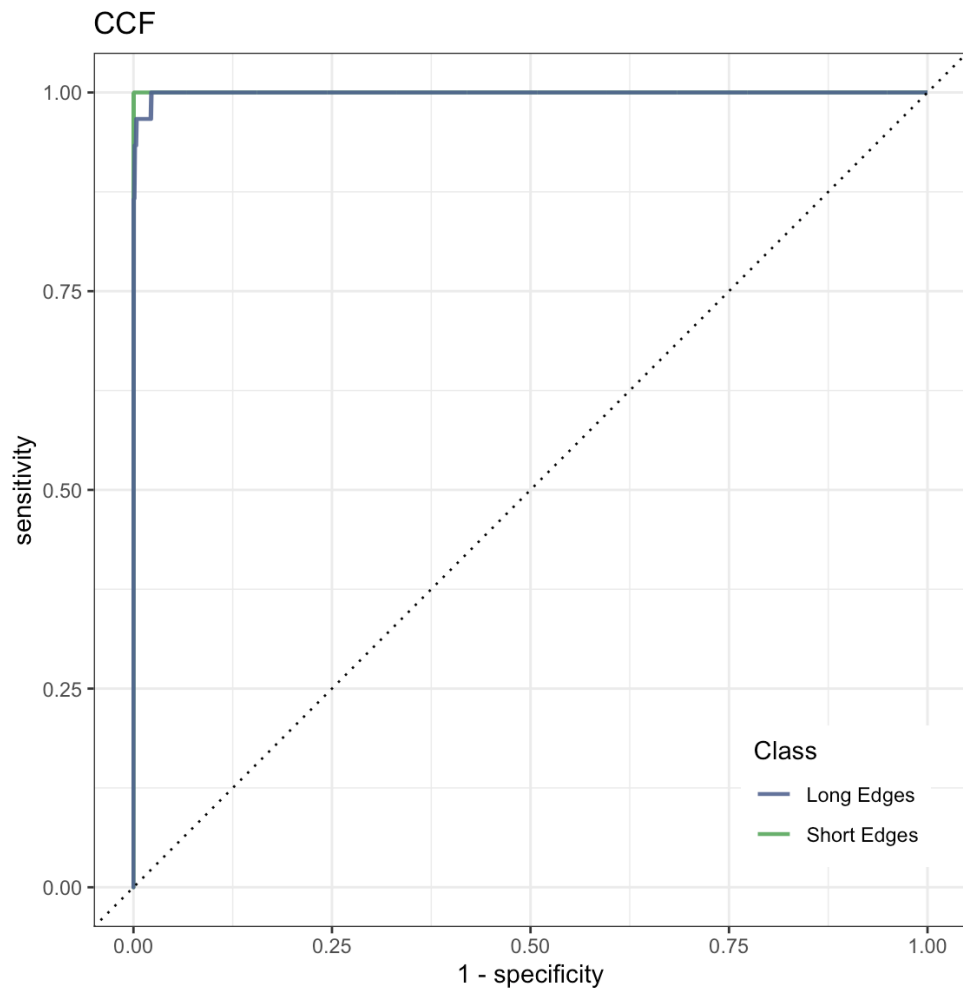


Figure 8. The ROC curve is bending very close to the upper left corner, which means excellent in classification and drawing conclusions.

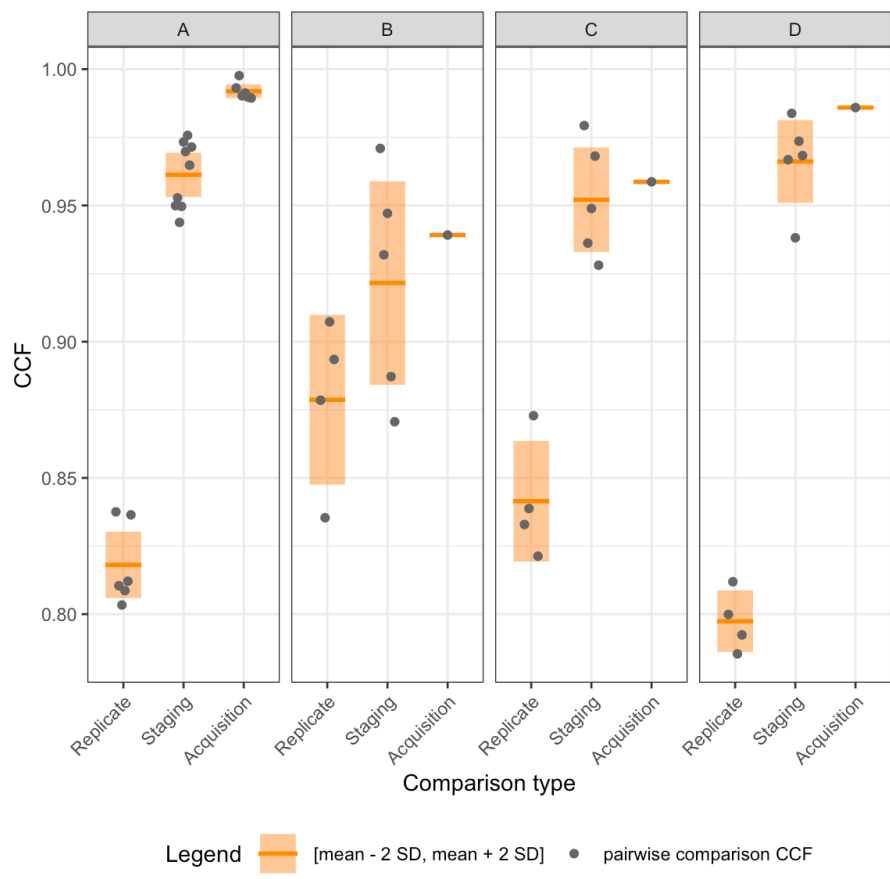


Figure 9

Table 3. Overview of available codes.

	Description	Section
Inspect raw scans		
1-create_pngs_from_x3p.R	obtain images of x3ps in scans /	Cutting Wires
Extract profiles		
2-create_profiles_from_x3p.R	manually extract profiles from each scan	Extract Profiles
3-create-single-profile-file.R	create meta profile information	Extract Profiles
Derive signals		
4-create_signals_from_profiles.R	derive signals from each profile	Filtered Signals
Align signals		
5-create-images.R	create images for pairwise alignment	Align Signals
6-align-pairwise.R	compute pairwise alignment CCF values	Align Signals
7-all-comparison-results.R	visualize comparison results	Align Signals

147 Usage Notes

148 The R package `x3ptools`¹⁶ available from CRAN supports working with files in `x3p` format. The sample scripts in R
149 for processing scans from `x3p` format to their signal and alignment are available on GitHub [heike/wirecuts-data](#) in the
150 assessment/code folder, as described in Table 3.

151 We already conduct pairwise comparisons and visualize some of the comparison results in Align Signals and Technical
152 Validation, and other analysis plots as well.

153 Suppose we put the CCF values in a tilemap with different tools, locations and edge combinations. In that case, we expect
154 only the diagonal to have high CCF values, close to 1 and marked as orange in the tilemap, as the diagonal represents the
155 same source, and the rest of the matrix to have low CCF values, close to 0 and marked as gray. In Figure 10, the behavior is
156 consistent with our expectation overall, except for some rare cases with tool 5 edge D. The density plot in Figure 11 shows the
157 distribution of the CCF values with the same sources and different sources. The overlapping points between the tails of these
158 two distributions to be a rough threshold.

159 Furthermore, the ROC curve in Figure 8 shows the sensitivity / true positive rate against the false positive rate (FPR) (1 -
160 specificity). The curve is very close to the upper left corner, which is excellent for classification and drawing conclusions. It
161 gives us a true threshold of 0.589 to control the FPR to be less than 0.05 with a false negative rate (FNR) to be 0, (false positive
162 rate (FPR) / false discovery rate (FDR) -> define the H0 or call it false identification rate (FIR)??), and 0.658 to control the
163 FPR to be less than 0.01, with FNR to be 0.02.

164 Code availability

165 We made available all codes we used for inspecting raw scans, extracting profiles, deriving signals, aligning signals, and visualizing
166 comparison results discussed in Methods and Technical Validation, as described in Table 3. All results are reproducible
167 using these codes provided.

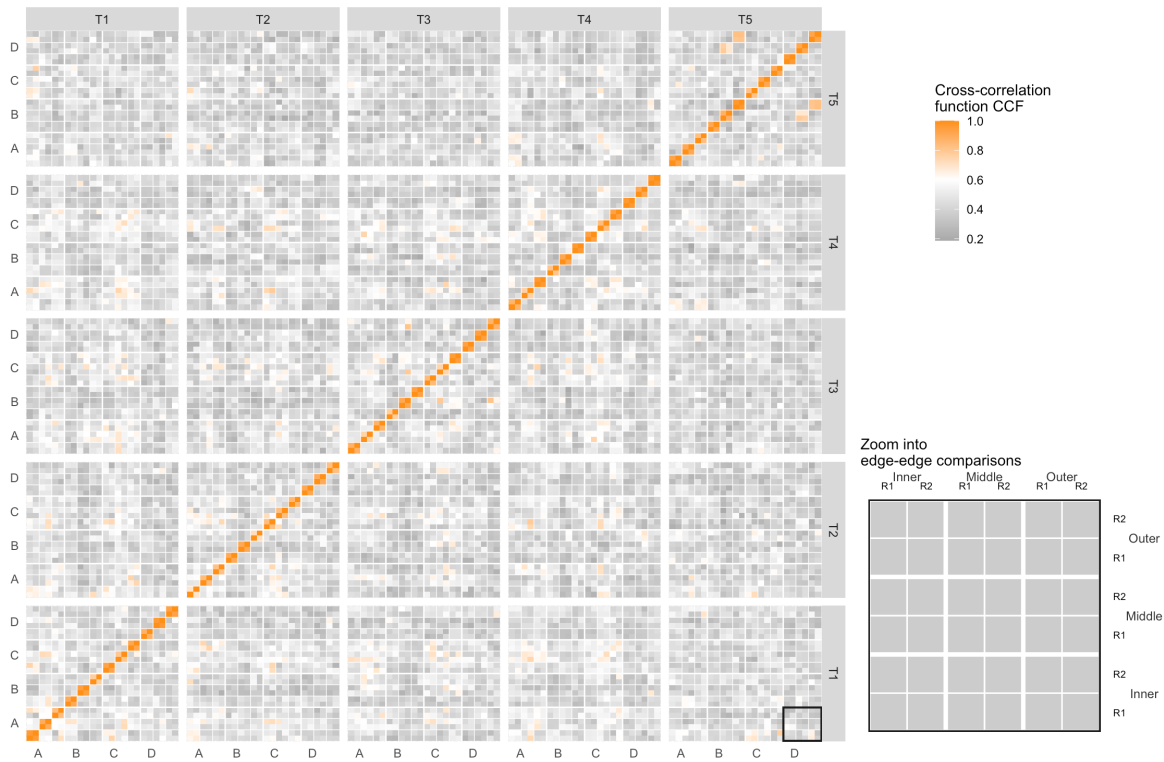


Figure 10. The tilemap shows signals from the same source have CCFs close to 1.

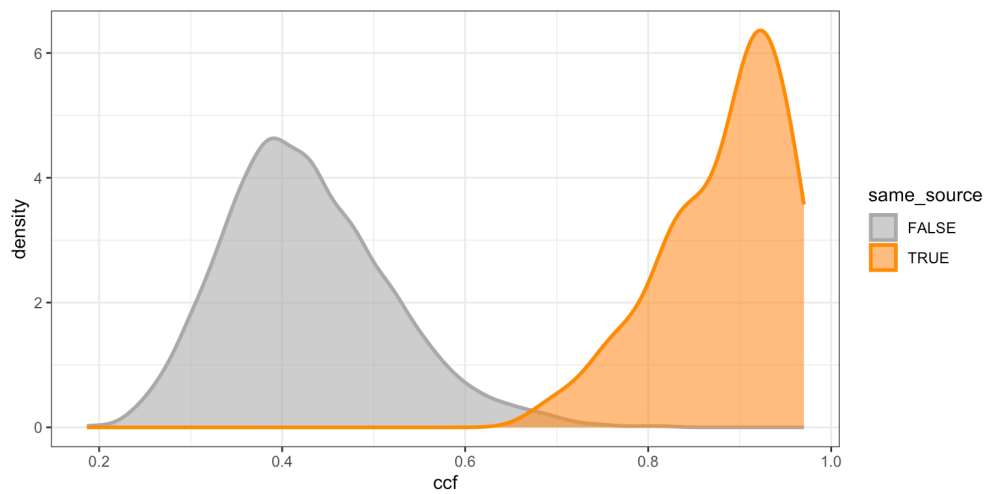


Figure 11. The density plot shows tails of distributions overlap, which to be used as a rough threshold for drawing conclusions.

168 References

- 169 1. Lindley, D. V. A Problem in Forensic Science. *Biometrika* **64**, 207, [10.2307/2335686](https://doi.org/10.2307/2335686) (1977). [2335686](#).
- 170 2. AFTE. The association of firearm and tool mark examiners: Theory of identification as it relates to toolmarks. *AFTE J.* **30**, 86–88 (1998).
- 171 3. NRC. *National Research Council: Strengthening Forensic Science in the United States: A Path Forward* (National Academies Press, 2009).
- 172 4. President's Council of Advisors on Science and Technology. *President's Council of Advisors on Science and Technology: Forensic Science in Criminal Courts: Ensuring Scientific Validity of Feature-Comparison Methods* (Executive Office of the President of the United States, President's Council, Washington, D.C., 2016).
- 173 5. Biedermann, A. The strange persistence of (source) “identification” claims in forensic literature through descriptivism, diagnosticism and machinism. *Forensic Sci. Int. Synerg.* **4**, 100222, [10.1016/j.fsisyn.2022.100222](https://doi.org/10.1016/j.fsisyn.2022.100222) (2022).
- 174 6. Baiker, M., Pieterman, R. & Zoon, P. Toolmark variability and quality depending on the fundamental parameters: Angle of attack, toolmark depth and substrate material. *Forensic Sci. Int.* **251**, 40–49, [10.1016/j.forsciint.2015.03.003](https://doi.org/10.1016/j.forsciint.2015.03.003) (2015).
- 175 7. Garcia, D. L., Pieterman, R. & Baiker, M. Influence of the axial rotation angle on tool mark striations. *Forensic Sci. Int.* **279**, 203–218, [10.1016/j.forsciint.2017.08.021](https://doi.org/10.1016/j.forsciint.2017.08.021) (2017).
- 176 8. Cuellar, M., Gao, S. & Hofmann, H. An algorithm for forensic toolmark comparisons. *Forensic Sci. Int. Synerg.* **9**, 100543, [10.1016/j.fsisyn.2024.100543](https://doi.org/10.1016/j.fsisyn.2024.100543) (2024).
- 177 9. Ma, L. *et al.* NIST Bullet Signature Measurement System for RM (Reference Material) 8240 Standard Bullets. *J. Forensic Sci.* **49**, 1–11, [10.1520/JFS2003384](https://doi.org/10.1520/JFS2003384) (2004).
- 178 10. Zheng, X. A., Soons, J. A. & Thompson, R. M. NIST Ballistics Toolmark Research Database | NIST (2016).
- 179 11. Chu, W., Thompson, R. M., Song, J. & Vorburger, T. V. Automatic identification of bullet signatures based on consecutive matching striae (CMS) criteria. *Forensic Sci. Int.* **231**, 137–141, [10/gn65cz](https://doi.org/10/gn65cz) (2013).
- 180 12. Vorburger, T. *et al.* Applications of cross-correlation functions. *Wear* **271**, 529–533, [10.1016/j.wear.2010.03.030](https://doi.org/10.1016/j.wear.2010.03.030) (2011).
- 181 13. Hare, E., Hofmann, H., Carriquiry, A. *et al.* Automatic matching of bullet land impressions. *The Annals Appl. Stat.* **11**, 2332–2356, [10.1214/17-AOAS1080](https://doi.org/10.1214/17-AOAS1080) (2017).
- 182 14. Ju, W. & Hofmann, H. The R Journal: An Open-Source Implementation of the CMPS Algorithm for Assessing Similarity of Bullets. *The R J.* **14**, 267–285, [10.32614/RJ-2022-035](https://doi.org/10.32614/RJ-2022-035) (2022).
- 183 15. Cleveland, W. S., Grosse, E. & Shyu, W. M. Local Regression Models. In *Statistical Models in S* (Routledge, 1992).
- 184 16. Hofmann, H., Vanderplas, S., Krishnan, G. & Hare, E. X3ptools: Tools for Working with 3D Surface Measurements, [10.32614/CRAN.package.x3ptools](https://doi.org/10.32614/CRAN.package.x3ptools) (2018).

198 Acknowledgements

199 This work was partially funded by the Center for Statistics and Applications in Forensic Evidence (CSAFE) through Cooperative
200 Agreement 70NANB20H019 between NIST and Iowa State University, which includes activities carried out at Carnegie
201 Mellon University, Duke University, University of California Irvine, University of Virginia, West Virginia University, University
202 of Pennsylvania, Swarthmore College and the University of Nebraska-Lincoln.

203 Author contributions statement

204 Let's follow the Elsevier definitions: <https://www.elsevier.com/researcher/author/policies-and-guidelines/credit-author-statement>
205 Y.L.: Methodology, Software, Validation, Data Curation, Writing - Draft; H.H.: Conceptualization, Methodology, Validation,
206 Writing - Review & Editing; C.M.: Lab supervision; E.A.: Physical Specimen, Scanning; J.S: Forensic advice; A.C.: Funding acquisition.
207
208 All authors reviewed the manuscript.

209 **Competing interests**

210 (mandatory statement)

211 H.H. is a technical advisor to AFTE (Association of Firearms and Toolmarks Examiners), fellow of the ASA (American
212 Statistical Association), and committee member of the ASA Forensic Science Committee. H.H. has testified as court witness
213 on behalf of judge April Neubauer, NY State Supreme Court Criminal Term in New York City. [other competing interests -](#)
214 [Alicia?](#)